ChemPubSoc Europe

DOI: 10.1002/cctc.201900095

CHEMCATCHEM Full Papers

Facile Preparation of 1T/2H-Mo($S_{1-x}Se_x$)$_2$ Nanoparticles for Boosting Hydrogen Evolution Reaction

Zhiping Lin[+],[a, b] Bo Lin[+],[b] Zongpeng Wang,*[a] Shougang Chen,*[b] Chengwei Wang,[b] Mengyao Dong,[d, f] Qiang Gao,*[c] Qian Shao,[e] Tao Ding,*[g] Hu Liu,[d, f] Shide Wu,[h] and Zhanhu Guo*[d]

2D transition metal dichalcogenides with a formula MoX_2 (X = S or Se) have been explored as promising earth-abundant catalysts for hydrogen evolution reaction (HER), especially those with 1T phases. Theoretical calculations and experiments have indicated that optimal catalytic performance can be achieved by regulating the atomic ratio of S and Se in Mo($S_{1-x}Se_x$)$_2$. However, the preparation of 1T phase Mo($S_{1-x}Se_x$)$_2$ is challenging because of the differences of S and Se elements. Here, we propose a facile and effective hydrothermal method for the production of 1T/2H Mo($S_{1-x}Se_x$)$_2$, with which products with various x values are prepared. The as-prepared Mo($S_{1-x}Se_x$)$_2$ samples give a low Tafel slope of 42.8 mV dec^{-1} (x = 0.25), and an overpotential of 161 mV (x = 0.5), which are state-of-the-art among the tremendous MoX_2 works. The excellent electrocatalytic performance is derived from the coexistence of S and Se atoms which reduces the reaction potential energy, and the presence of the 1T phase which improves the conductivity. Additionally, the ratio of 1T phase to 2H phase of Mo($S_{1-x}Se_x$)$_2$ is found controllable over reaction temperature.

Introduction

Serious consumption of fossil fuels leading to severe energy crisis and environmental pollution has stimulated our society to seek green energy sustainability.[1] Accordingly, we have witnessed extensive research on enhanced energy related technologies, such as batteries,[2] supercapacitors,[3] fuel cells,[4] etc. On the other hand, energy carrier-Hydrogen, a so-called future energy fuel, can be effectively obtained by water electrolysis through hydrogen evolution reaction (HER).

To produce hydrogen efficiently, electrocatalysts with good catalytic activity are of extremely importance. Thus far, precious platinum (Pt) has been considered to be the best HER catalyst with decent catalytic activity and high stability.[1b] To realize cost-effective production of H_2, last decade has witnessed the rapid expansion of precious-metal-free HER catalysts with comparable performance to Pt, including transition metal sulfides,[5] selenides,[5d,6] carbides[7] and phosphides,[8] etc. Amongst, molybdenum disulfides with a formula MoX_2 (X = S or Se) have drawn the most remarkable attention due to their good catalytic activity and regulatable properties.[5d,9] First-principles calculations have confirmed that MoX_2 materials exhibit near-but-none-zero hydrogen adsorption free energy (ΔG_H), which is highly desirable to achieve highest catalytic activity for HER. Meanwhile, theoretical calculations manifest that adsorption of H atoms to Mo edges in MoS_2 is weak (ΔG_H = +80 meV),[10] while that in $MoSe_2$ is strong (ΔG_H = −140 meV).[11] Therefore, it holds the promise to achieve

[a] Dr. Z. Lin,[+] Dr. Z. Wang
Department of Chemistry and Material Engineering
School of Advanced Study
Taizhou University
Taizhou 318000 (P.R. China)
E-mail: wangzp@tzc.edu.cn
[b] Dr. Z. Lin,[+] B. Lin,[+] Prof. S. Chen, C. Wang
Institute of Materials Science and Engineering
Ocean University of China
Qingdao 266100 (P.R. China)
E-mail: sgchen@ouc.edu.cn
[c] Dr. Q. Gao
Department of Heterogeneous Reaction, Max Planck Institute for Chemical Energy Conversion
45470 Mülheim an der Ruhr (Germany)
E-mail: gaoq@ornl.gov
[d] M. Dong, Dr. H. Liu, Prof. Z. Guo
Integrated Composites Laboratory, Department of Chemicl & Biomolecular Engineering
University of Tennessee
Knoxville, TN 37996 (USA)
E-mail: zguo10@utk.edu
[e] Q. Shao
College of Chemical and Environmental Engineering
Shandong University of Science and Technology
Qingdao 266590 (P.R. China)
[f] M. Dong, Dr. H. Liu
Key Laboratory of Materials Processing and Mold (Zhengzhou University), Ministry of Education
National Engineering Research Center for Advanced Polymer Processing Technology
Zhengzhou University
Zhengzhou 450002 (P.R. China)
[g] Prof. Dr. T. Ding
College of Chemistry and Chemical Engineering
Henan University
Kaifeng 475004 (P.R. China)
E-mail: dingtao@henu.edu.cn
[h] Prof. S. Wu
Henan Provincial Key Laboratory of Surface and Interface Science
Zhengzhou University of Light Industry
Zhengzhou 450001 (China)
[+] Zhiping Lin and Bo Lin contributed equally to this work.

Supporting information for this article is available on the WWW under https://doi.org/10.1002/cctc.201900095

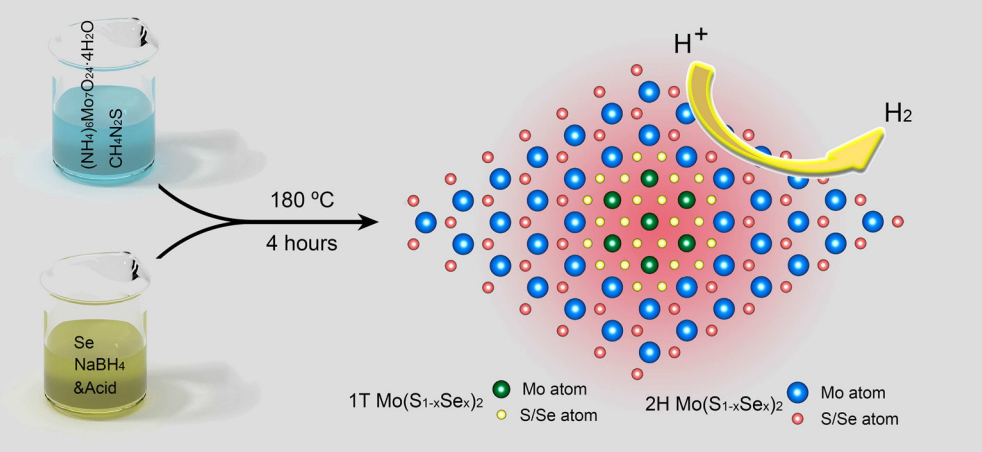

Figure 1. Schematic of the preparation of 1T/2H- $Mo(S_{1-x}Se_x)_2$.

thermoneutral hydrogen adsorption free energy by regulating the atomic ratio of S and Se in an alloy $Mo(S_{1-x}Se_x)_2$, thereby improving HER activity.[10] Experiments and computational theories have confirmed that selenization of MoS_2 can effectively improve its electrocatalytic performance.[12]

Due to the differences in the chemical and physical properties of S and Se, $Mo(S_{1-x}Se_x)_2$ nanoalloys can be mainly synthesized by approaches involving high temperatures, *e.g.,* CVD at above 800 °C[12c–f] or a complex organic solution method at 300 °C plus annealing at 400 °C.[10] However, the usage of high temperatures is against the spirit of green and sustainable energy. On the basis of thermodynamics, 2H phase MoX_2 is more stable than 1T phase,[9c] whereas previous reports on the preparation of $Mo(S_{1-x}Se_x)_2$ mainly focused on 2H phase with rare reports on 1T phase. When it comes to HER, the 1T phase MoX_2 is much more favorable than its 2H phase counterpart,[13] the catalytic potential of which is blocked by poor electrical conductivity and electrocatalytic inactivity of the basal plane.[9a,b, 14] Hence, the preparation of 1T/2H phase $Mo(S_{1-x}Se_x)_2$ nanoparticles at low temperature and high yield is highly demanded for practical application, which is currently rarely reported.

Herein, we have proposed and demonstrated a simple one-step hydrothermal method to prepare 1T/2H phase $Mo(S_{1-x}Se_x)2$ nanoparticles with regulated x values. To obtain the thermodynamically metastable 1T phase, appropriate amount of NaBH4 is utilized to dissolve Se powders under acidic conditions (as shown in Figure 1), and the temperature is relatively low to hinder the formation of 2H phase. The $x=0.5$ $Mo(S_{1-x}Se_x)2$ exhibits an overpotential of 161 mV vs RHE at $j=-10$ mA cm^{-2} and a Tafel slope of 52.0 mV dec^{-1}. MoS1.5Se0.5 exhibits an extremely low Tafel slope of 42.8 mV dec^{-1}, outperforming most previously reported MoX2. Furthermore, the ratio of 1T phase to 2H phase of Mo(S1-xSex)2 depends essentially on reaction temperature, indicating the versatility of the proposed method. The proposed method possesses the characteristics of easy, productive, and low temperature throughout the entire process, greatly promoting the possibility of the practical applications.

Results and Discussion

A series of $Mo(S_{1-x}Se_x)_2$ ($x=0$, 0.25, 0.5, 0.75, 1) samples are successfully synthesized through hydrothermal synthesis method to explore the HER electrocatalytic activity in acid solution (Figure 1). Powder X-ray diffraction pattern (PXRD) is performed to investigate the structural features of the samples. For both samples, the XRD patterns (Figure 2a) show the characteristic peaks of 2H phase (JCPDS 37-1492 for 2H-MoS_2 and JCPDS 29-0914 for 2H-$MoSe_2$). The representative peaks (002), (100) and (110) shift gradually to lower angle with increasing *x*, owing to the larger radius of Se ion than that of the S ion. The broadening diffraction peaks of the samples arose from the crystallization of the samples,[5a] confirmed by the later electron microscope experiment. The diffraction peaks of 1T phase is not observed because of the similar positions of diffraction peaks between 1T phase and 2H phase and the broadening of the diffraction peaks.[15]

Phase composition and alloy composition of $Mo(S_{1-x}Se_x)_2$ nanoparticles have been further investigated by Raman spectroscopy. Two vibration modes (~282 cm^{-1} and ~376 cm^{-1}) are assigned to the $E_{1g(S\text{-}Mo)}$ and $E_{2g(S\text{-}Mo)}$ molecular vibration modes of 2H-MoS_2, respectively (Figure 2b).[6a] The vibration peak ~282 cm^{-1} gradually shifts to a low frequency region as *x* increases in $Mo(S_{1-x}Se_x)_2$ nanoparticles. Moreover, several vibration modes (~236 and ~336 cm^{-1}) of 1T-MoS_2 and (~354 and ~484 cm^{-1}) of 1T-$MoSe_2$ demonstrated the coexist of 2H phase and 1T phase (Figure 2b).[15b]

TEM is further used to measure the structural characteristics of MoSSe ($x=0.5$) sample as a representative example of $Mo(S_{1-x}Se_x)_2$ nanoparticles. MoSSe nanoparticles present the grain size from 20 to 30 nm (Figure 2c). HRTEM shows that MoSSe nanoparticles consist of 2 to 4 atomic layers (Figure 2d). The distance between two adjacent atomic layers is about 0.76 nm, indicating extended atomic spacing of (002) planes of the 1T-MoSSe. The spacing between two adjacent atomic layers is approximately 0.64 nm, representing the structural features of (002) planes of 2H-MoSSe. The selected area electron diffraction

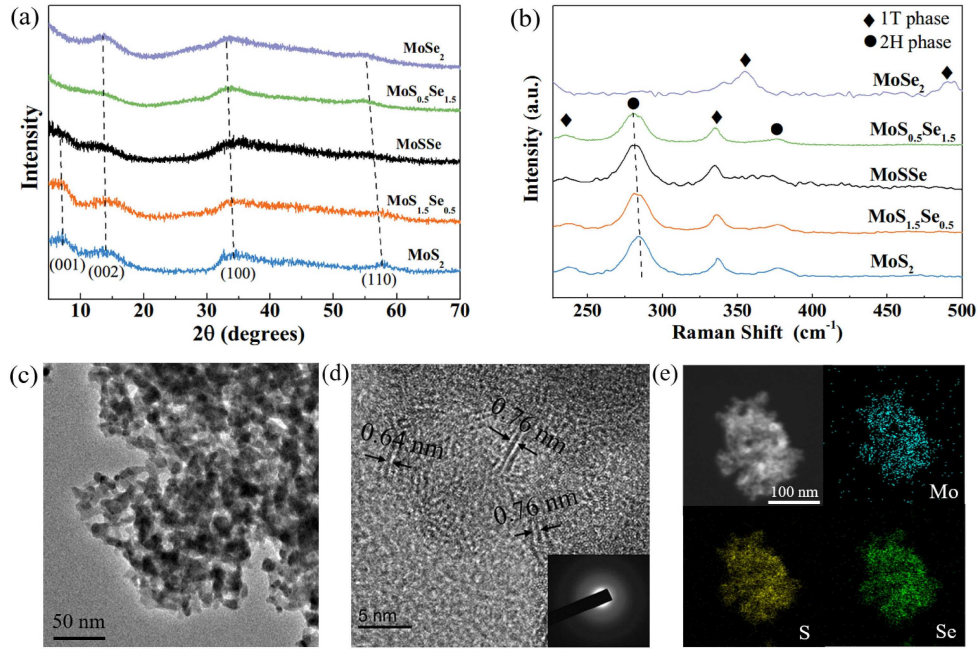

Figure 2. (a) PXRD patterns of $Mo(S_{1-x}Se_x)_2$ (x = 0, 0.25, 0.5, 0.75, 1) samples. (b) Raman spectra of $Mo(S_{1-x}Se_x)_2$ (x = 0, 0.25, 0.5, 0.75, 1) samples. (c) TEM of MoSSe sample. (d) HRTEM image of MoSSe sample. The inset is SAED pattern. (e) Element mapping images of MoSSe sample.

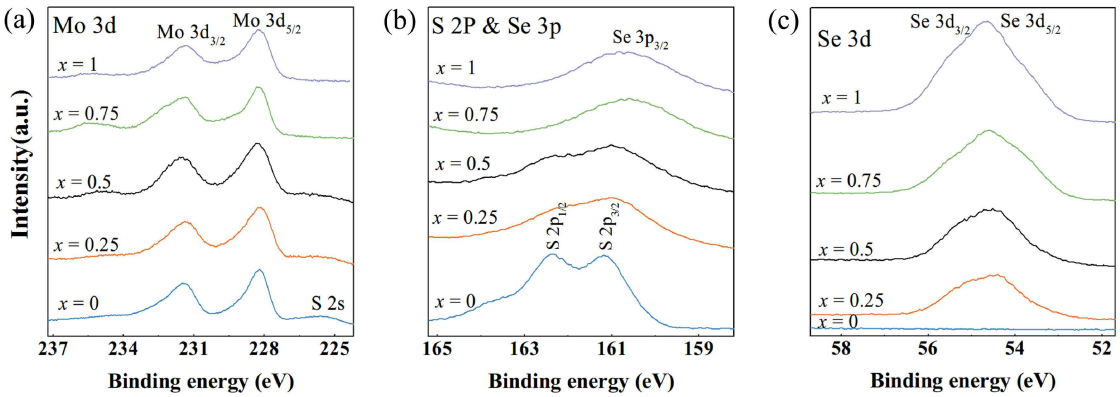

Figure 3. (a) High-resolution Mo 3d XPS spectra of $Mo(S_{1-x}Se_x)_2$ (x = 0, 0.25, 0.5, 0.75, 1) samples. (b) High-resolution S 2p & Se 3p XPS spectra of $Mo(S_{1-x}Se_x)_2$ (x = 0, 0.25, 0.5, 0.75, 1) samples. (c) High-resolution Se 3d XPS spectra of $Mo(S_{1-x}Se_x)_2$ (x = 0, 0.25, 0.5, 0.75, 1) samples.

pattern (SAED) indicates MoSSe sample is partially crystallized (inset of Figure 2d). The typical TEM bright field image and element mapping images of MoSSe sample (Figure 2e) shows that Mo, S and Se are uniformly and homogeneously distributed across the nanoparticles.

To further quantify the chemical compositions and phase compositions, X-ray photoelectron spectroscopy (XPS) has been employed for $Mo(S_{1-x}Se_x)_2$ ($x = 0$, 0.25, 0.5, 0.75, 1) samples (Figure 3 & S1 & S2). The peaks of Mo $3d_{3/2}$ and Mo $3d_{5/2}$ locate at 232.1 and 228.9 eV manifest the formation of Mo^{4+} of 2H phase. The two peaks located at 231.2 and 228.1 eV, which are shifted by approximately 0.9 eV to a lower bonding compared to the peaks of 2H phase, confirm the existence of the 1T phase.[16] The phase contents of 1T and 2H can be obtained from deconvolution of the Mo 3d peaks (Table S1). All $Mo(S_{1-x}Se_x)_2$ ($x = 0$, 0.25, 0.5, 0.75, 1) samples contain about 50 percent of 1T phase and 50 percent of 2H phase. As the amount of Se increases, the intensity of S 2p peak gradually decreases until completely disappears when $x = 1$(Figure 3b & S2). The atomic ratios of S and Se of $Mo(S_{1-x}Se_x)_2$ ($x = 0$, 0.25, 0.5, 0.75, 1) samples can be calculated by the formula: $Se/S = (I_{Se} * F_S)/(I_S * F_{Se})$ from the S 2p and Se 3p peaks (Table S1). I_{Se} and I_S are the areas of the peaks of Se $3p_{3/2}$ and S $2p_{3/2}$. F_{Se} and F_S represent the relative symmetric factors (R.S.F) for Se $3p_{3/2}$ (0.4453) and S $2p_{3/2}$ (0.8493), respectively.[17] The obtained actual atomic ratios are close to the nominal ratios. With the increase of Se content, the peak of Se 3d gradually increases (Figure 3c), which agrees with the analysis in Figure 3b. Through the detailed characterization and analysis of Raman, HRTEM and XPS results, we confirmed the existence of the 1T phase $Mo(S_{1-x}Se_x)_2$ hold the great

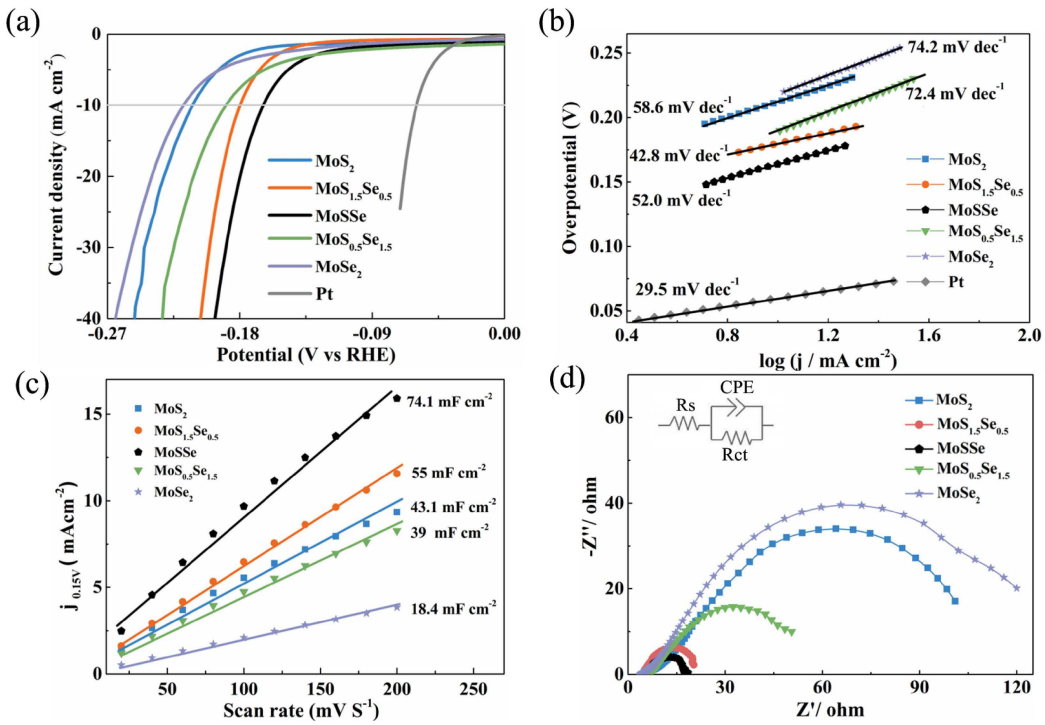

Figure 4. Electrochemical HER measurements of $Mo(S_{1-x}Se_x)_2$ (x = 0, 0.25, 0.5, 0.75, 1) samples. (a) IR-corrected linear sweep polarization curves measured in 0.5 M H_2SO_4. (b) The corresponding Tafel slopes. (c) The corresponding extraction of Cdl slopes. (d) The electrochemical impedance diagrams.

promise for metal property and better electrocatalytic activity than 2H phase, which will further improve the electrocatalytic activity for HER.

To explore the coexistence of S and Se atoms, the electrochemical HER measurements of $Mo(S_{1-x}Se_x)_2$ ($x = 0$, 0.25, 0.5, 0.75, 1) samples were evaluated with 0.50 M H_2SO_4(Figure 4). Summary of the electrocatalytic performance parameters for various $Mo(S_{1-x}Se_x)_2$ samples is shown in Table S1. MoS_2, $MoS_{1.5}Se_{0.5}$, MoSSe, $MoS_{0.5}Se_{1.5}$ and $MoSe_2$ samples can attain a current density of $-10\ mA\,cm^{-2}$ at overpotentials of 210, 178, 161, 188 and 216 mV vs RHE after iR correction, respectively. From the extrapolation of the linear region of overpotential versus log j (Figure 4b), the corresponding Tafel slopes of 58.6, 42.8, 52.0, 72.4 and 74.2 $mV\,dec^{-1}$ (after iR correction) are obtained for MoS_2, $MoS_{1.5}Se_{0.5}$, MoSSe, $MoS_{0.5}Se_{1.5}$ and $MoSe_2$ samples, respectively. When $0 \le x \le 0.5$, as the Se content increases, the overpotentials of $Mo(S_{1-x}Se_x)_2$ gradually decrease. When $0.5 \le x \le 1$, the overpotentials of $Mo(S_{1-x}Se_x)_2$ increase with increasing Se content. It has been reported that MoSSe obtained by high temperature CVD can achieve a catalytic current density of $-10\ mA\,cm^{-2}$ at an overpotential of 219 mV, with a Tafel slope of 55 $mV\,dec^{-1}$.[12e] Note that the overpotential (161 mV vs RHE) and Tafel slop (52.0 $mV\,dec^{-1}$) of MoSSe obtained here outperformed previous reports of $Mo(S_{1-x}Se_x)_2$.[10,12c–f] The as-prepared $MoS_{1.5}Se_{0.5}$ exhibits an extremely low Tafel slope of 42.8 $mV\,dec^{-1}$, which is state-of-the-art among the tremendous reported MoX_2 (Table S2). The excellent electrocatalytic performance is derived from the coexistence of S and Se atoms which reduces the reaction potential energy. It is possible to achieve thermoneutral hydrogen adsorption free energy by regulating the atomic ratio of S and Se in the alloy $Mo(S_{1-x}Se_x)_2$ and consequently realized the best HER activity. Based on in-depth investigation of the naturally electrocatalytic activity, the double-layer capacitance (C_{dl}) derived from the cyclic voltammetry (CV, Figure S3) and electrochemical impedance spectroscopy (EIS) curves are shown in Figure 4c and 4d. The double-layer capacitance (C_{dl}) is used to evaluate the electrochemical catalytic active area of as-prepared materials based on the general assumption that the materials have the same geometric sizes and surface areas. From CV (Figure S3), the corresponding C_{dl} of 43.1, 55.0, 74.1, 39.0 and 18.4 $mF\,cm^{-2}$ (after iR correction) are obtained for MoS_2, $MoS_{1.5}Se_{0.5}$, MoSSe, $MoS_{0.5}Se_{1.5}$ and $MoSe_2$ samples, respectively. Amongst $Mo(S_{1-x}Se_x)_2$ materials, MoSSe has the max C_{dl} values (74.1 $mF\,cm^{-2}$), indicating that MoSSe sample has the largest active surface area. As shown in Figure 4d and Table S1, the charge transfer resistance (R_{ct}) of MoSSe catalyst is less than other samples, suggesting that MoSSe facilitated charge transfer during HER. Moreover, linear sweep polarization curves for MoSSe shown negligible attenuation after 1,000 cycles (Figure S4), indicating the high stability in strongly acidic medium. Time dependence current density under a static overpotential of 161 mV further confirmed the stability of MoSSe (Figure S5). The characterizations of MoSSe sample was also performed after cycling test. According to the XRD pattern (Figure S6), Raman spectrum (Figure S7), XPS spectrum (Figure S8) and TEM image (Figure S9), it is evident that MoSSe sample has little changed after the cycling test.

To further explore the role of the 1T phase and the 2H phase of $Mo(S_{1-x}Se_x)_2$ for HER, we tried to adjust the ratio of the content of the two phases. It is found that the phase ratio of 1T to 2H in $Mo(S_{1-x}Se_x)_2$ can be regulated by controlling the reaction temperatures. As MoSSe ($x=0.5$) gives the lowest overpotential, we employed it to perform the phase content investigation. The phase contents of 1T and 2H can be obtained from deconvolution of the Mo 3d peaks (Figure S10 and Table S3). With increasing temperatures, the content of 1T phase gradually increased to a maximum of 51.2% at the temperature of 180 °C in the range from 140 °C to 180 °C, and then decreased to 38.9% at 200 °C (Table S3), indicating a comparably high temperature may convert partial 1T phase back into 2H phase.[13c,16] Correspondingly, the electrocatalytic performance of MoSSe becomes better with increasing temperature from 140 °C to 180 °C (Table S3). The electrocatalytic ability of MoSSe samples obtained ranging from 140 °C to 200 °C is shown in Figure S11, S12 and Table S3. At 180 °C, MoSSe has the best electrocatalytic properties, including the lowest overpotential at $j=-10\ mA\,cm^{-2}$ and Tafel slope, because the highest phase content of 1T phase can be formed. And as the temperature increases further, the performance decreases. The excellent electrocatalytic performance is derived from the high content of the 1T phase, which is a metal phase with higher conductivity (Figure S7).

Conclusions

In summary, we have demonstrated a facial one-step hydrothermal method for the production of 1T/2H phase $Mo(S_{1-x}Se_x)_2$ nanoparticles, which bypassed the problem of high temperatures encountered in other approaches. Various samples with different x values were prepared and their electrochemical HER catalytic activity were examined. Amongst, $MoS_{1.5}Se_{0.5}$ exhibits the lowest Tafel slope of $42.8\ mV\,dec^{-1}$, while MoSSe gives the best overpotential of 161 mV at $10\ mA\,cm^{-2}$. The HER activity is state-of-the-art among the tremendous MoX_2 works. Furthermore, the phase content of $Mo(S_{1-x}Se_x)_2$ can be modulated by simply controlling the synthesis temperatures. The excellent electrocatalytic performance is derived from the coexistence of S and Se atoms which reduces the reaction potential energy, and the presence of the 1T phase improved the conductivity. Utilizing the proposed method, 1T/2H $Mo(S_{1-x}Se_x)_2$ catalysts can be prepared in large scale with low cost, high efficiency and stability, which will boost the practical applications of MoX_2-group catalysts.

Experimental Section

Synthesis. $(NH_4)_6Mo_7O_{24}\cdot 4H_2O$ (99%), thiourea CH_4N_2S (99%), selenium powder (99%), sodium borohydride $NaBH_4$ (98%) and glacial acetic acid CH_3COOH (99.5%) were purchased in Sinopharm Chemical Reagent Co.,Ltd. Typically, 0.1 mmol $(NH_4)_6Mo_7O_{24}\cdot 4H_2O$ and 3 mmol CH_4N_2S were mixed together and then dissolved in 20 mL distilled water. We used magnetic stirring to get the homogeneous solution of 1 mmol Se and 3 mmol $NaBH_4$, and then the solution was adjusted to be acid by CH_3COOH. These two solutions were placed in 50 mL Teflon-lined stainless-steel autoclave. The autoclave was kept at a certain temperature for 4 hours to ensure the chemical reaction completely, as shown in Figure 1. The obtained products were cleaned by distilled water and ethyl alcohol for three times to remove the impurities. Finally, the as-formed products were freeze dried under vacuum. Various $MoS_{1-x}Se_x$ samples with different molar ratios of Sulphur source and Selenium resource were obtained following the same procedure.

Characterization. Powder X-ray diffraction data (XRD) was collected on a Bruker-D8 Advance with Cu Ka radiation and a graphite monochromator. Transmission electron microscopy (TEM) images were observed by TESCAN VEGA3 (TESCAN, Czech). The high-resolution TEM (HRTEM) was carried out on a JEOL JEM-ARF2100F TEM/STEM. The X-ray photoelectron spectroscopy (XPS) was conducted on Thermo Fisher Scientific ESCALAB 250 Xi using Al Ka ($h\nu = 1486.6$ eV) radiation source. The Raman spectra was conducted on Thermo DXR Raman Microscope using 532 nm laser.

Electrochemical Tests. All electrochemical measurements were conducted on the electrochemical workstation (CHI 760E) by a conventional three-electrode method at the temperature of 30 °C. Samples were loaded on a glassy carbon electrode (GCE, 3 mm diameter, $0.07068\ cm^2$) as the working electrode. An Ag/AgCl electrode was chosen as the reference electrode and a graphite rod as the counter electrode. The catalyst solutions were prepared by mixing 5 mg catalysts in a solution containing 774 μL deionized water, 194μL alcohol, and 32 μL 5 wt % Nafion solution by sonication for 0.5 hour. Then, 12.5 μL of well-dispersed catalyst solution were dropped on the surface of GCE, followed by drying naturally. The HER performance was measured in N_2-saturated 0.5 M H_2SO_4 solution with a scan rate of $5\ mV\,s^{-1}$. All potentials were corrected with IR to a reversible hydrogen electrode (RHE). The corresponding Tafel slopes were calculated from linear polarization curves. Cyclic voltammetry (CV) measurements were recorded from 0.1 to 0.2 V versus RHE at a series of scan rates ranging from 20 to $200\ mV\,s^{-1}$ for evaluation of the double-layer capacities of the samples. EIS measurements were carried out from 100 kHz to 0.1 Hz under a static overpotential of 200 mV. The electrochemical durability was conducted by 1,000 cyclic voltammetry sweeps at $100\ mV\,s^{-1}$. Time dependence of the current density measurement was obtained under a static overpotential of 161 mV for 30000 seconds.

Acknowledgements

The authors acknowledge National Natural Science Foundation of China (51572249) and the Fundamental Research Funds for the Central Universities (841562011).

Conflict of Interest

The authors declare no conflict of interest.

Keywords: Hydrogen Evolution Reaction · Electrocatalysts · Hydrogen Energy · Catalytic Activity · 1T Phase · MoX_2

[1] a) J. A. Turner, *Science* **2004**, *305*, 972–974; b) S. Bai, C. M. Wang, M. S. Deng, M. Gong, Y. Bai, J. Jiang, Y. J. Xiong, *Angew. Chem. Int. Ed.* **2014**, *53*, 12120–12124; *Angew. Chem.* **2014**, *126*, 12316–12320; c) H. Yang, L.

Geng, Y. Zhang, G. Chang, Z. Zhang, X. Liu, M. Lei, Y. He, *Appl. Surf. Sci.* **2019**, *466*, 385–392; d) H. Wang, R. Liu, Y. Li, X. Lü, Q. Wang, S. Zhao, K. Yuan, Z. Cui, X. Li, S. Xin, R. Zhang, M. Lei, Z. Lin, *Joule* **2018**, *2*, 337–348; e) T. Su, Q. Shao, Z. Qin, Z. Guo, Z. Wu, *ACS Catal.* **2018**, *8*, 2253–2276; f) C. Wang, F. Lan, Z. He, X. Xie, Y. Zhao, H. Hou, L. Guo, M. Vignesh, Q. Shao, H. Liu, Q. Gao, T. Ding, Z. Guo, *ChemSusChem*, **2019**, in press, doi: 10.1002/cssc.201802873.

[2] a) J. Tian, Q. Shao, X. Dong, J. Zheng, D. Pan, X. Zhang, H. Cao, L. Hao, J. Liu, X. Mai, Z. Guo, *Electrochim. Acta* **2018**, *261*, 236–245; b) M. Liu, Z. Yang, H. Sun, C. Lai, X. Zhao, H. Peng, T. Liu, *Nano Res.* **2016**, *9*, 3735–3746; c) M. Liu, Y. Liu, Y. Yan, F. Wang, J. Liu, T. Liu, *Chem. Commun.* **2017**, *53*, 9097–9100; d) M. Liu, Q. Meng, Z. Yang, X. Zhao, T. Liu, *Chem. Commun.* **2018**, *54*, 5090–5093; e) C. Hou, Z. Tai, L. Zhao, Y. Zhai, Y. Hou, Y. Fan, F. Dang, J. Wang, H. Liu, *J. Mater. Chem. A* **2018**, *6*, 9723–9736; f) Z. Qu, M. Shi, H. Wu, Y. Liu, J. Jiang, C. Yan, *J. Power Sources* **2019**, *410*, 179–187; g) W. Zhao, X. Li, R. Yin, L. Qian, X. Huang, H. Liu, J. Zhang, J. Wang, T. Ding, Z. Guo, *Nanoscale* **2019**, *11*, 50–59; h) M. Idrees, S. Batool, J. Kong, Q. Zhuang, H. Liu, Q. Shao, N. Lu, Y. Feng, E. K. Wujcik, Q. Gao, T. Ding, R. Wei, Z. Guo, *Electrochim. Acta* **2019**, *296*, 925–937; i) R. Li, X. Zhu, Q. Fu, G. Liang, Y. Chen, L. Luo, M. Dong, Q. Shao, C. Lin, R. Wei, Z. Guo, *Chem. Commun.* **2019**, 55, 2493-2496; j) X. Lou, C. Lin, Q. Luo, J. Zhao, B. Wang, J. Li, Q. Shao, X. Guo, N. Wang, Z. Guo, *ChemElectroChem* **2017**, *4*, 3171–3180.

[3] a) M. Liu, B. Li, H. Zhou, C. Chen, Y. Liu, T. Liu, *Chem. Commun.* **2017**, *53*, 2810–2813; b) B. Kirubasankar, V. Murugadoss, J. Lin, T. Ding, M. Dong, H. Liu, J. Zhang, T. Li, N. Wang, Z. Guo, S. Angaiah, *Nanoscale* **2018**, *10*, 20414–20425; c) W. Du, X. Wang, J. Zhan, X. Sun, L. Kang, F. Jiang, X. Zhang, Q. Shao, M. Dong, H. Liu, V. Murugadoss, Z. Guo, *Electrochim. Acta* **2019**, *296*, 907–915.

[4] a) C. Wang, B. Mo, Z. He, Q. Shao, D. Pan, E. Wujick, J. Guo, X. Xie, X. Xie, Z. Guo, *J. Membr. Sci.* **2018**, *556*, 118–125; b) H. Du, C. X. Zhao, J. Lin, J. Guo, B. Wang, Z. Hu, Q. Shao, D. Pan, E. K. Wujcik, Z. Guo, *The Chemical Record* **2018**, *18*, 1365–1372.

[5] a) J. F. Xie, H. Zhang, S. Li, R. X. Wang, X. Sun, M. Zhou, J. F. Zhou, X. W. Lou, Y. Xie, *Adv. Mater.* **2013**, *25*, 5807–5813; b) M. R. Gao, M. K. Chan, Y. G. Sun, *Nat. Commun.* **2015**, *6*, 7493; c) L. Cheng, W. J. Huang, Q. F. Gong, C. H. Liu, Z. Liu, Y. G. Li, H. J. Dai, *Angew. Chem. Int. Ed.* **2014**, *53*, 7860–7863; *Angew. Chem.* **2014**, *126*, 7994–7997; d) R. Wang, J. C. Han, X. H. Zhang, B. Song, *J. Mater. Chem. A* **2018**, *6*, 21847–21858; e) L. Wang, X. Duan, G. Wang, C. Liu, S. Luo, S. Zhang, Y. Zeng, Y. Xu, Y. Liu, X. Duan, *Appl. Catal. B* **2016**, *186*, 88–96; f) K. Wang, J. Yang, J. Zhu, L. Li, Y. Liu, C. Zhang, T. Liu, *J. Mater. Chem. A* **2017**, *5*, 11236–11245; g) Q. He, L. Wang, K. Yin, S. Luo, *Nanoscale Res. Lett.* **2018**, *13*, 167; h) G. Zhou, Y. Shan, L. Wang, Y. Hu, J. Guo, F. Hu, J. Shen, Y. Gu, J. Cui, L. Liu, X. Wu, *Nat. Commun.* **2019**, *10*, 399.

[6] a) X. Chia, A. Ambrosi, Z. Sofer, J. Luxa, M. Pumera, *ACS Nano* **2015**, *9*, 5164–5179; b) F. H. Saadi, A. I. Carim, J. M. Velazquez, J. H. Baricuatro, C. C. McCrory, M. P. Soriaga, N. S. Lewis, *ACS Catal.* **2014**, *4*, 2866–2873; c) Y. F. Xu, M. R. Gao, Y. R. Zheng, J. Jiang, S. H. Yu, *Angew. Chem. Int. Ed.* **2013**, *52*, 8546–8550; *Angew. Chem.* **2013**, *125*, 8708–8712; d) Y. W. Liu, X. M. Hua, C. Xiao, T. F. Zhou, P. C. Huang, Z. P. Guo, B. C. Pan, Y. Xie, *J. Am. Chem. Soc.* **2016**, *138*, 5087–5092; e) A. Y. S. Eng, A. Ambrosi, Z. Sofer, P. Simek, M. Pumera, *ACS Nano* **2014**, *8*, 12185–12198; f) Z. P. Lin, C. W. Wang, Z. P. Wang, Q. Y. Liu, C. C. Le, B. Lin, S. G. Chen, *Electrochim. Acta* **2019**, *294*, 142–147; g) J. Yang, Y. Liu, C. Shi, J. Zhu, X. Yang, S. Liu, L. Li, Z. Xu, C. Zhang, T. Liu, *ACS Appl Energy Mater* **2018**, *1*, 7035–7045.

[7] a) Y. Liu, G. Yu, G. D. Li, Y. Sun, T. Asefa, W. Chen, X. Zou, *Angew. Chem. Int. Ed.* **2015**, *54*, 10752–10757; *Angew. Chem.* **2015**, *127*, 10902–10907; b) F. X. Ma, H. B. Wu, B. Y. Xia, C. Y. Xu, X. W. D. Lou, *Angew. Chem. Int. Ed.* **2015**, *54*, 15395–15399; *Angew. Chem.* **2015**, *127*, 15615–15619.

[8] a) L. A. Stern, L. G. Feng, F. Song, X. L. Hu, *Energy Environ. Sci.* **2015**, *8*, 2347–2351; b) A. Laursen, K. Patraju, M. Whitaker, M. Retuerto, T. Sarkar, N. Yao, K. Ramanujachary, M. Greenblatt, G. Dismukes, *Energy Environ. Sci.* **2015**, *8*, 1027–1034; c) Y. W. Tan, H. Wang, P. Liu, Y. H. Shen, C. Cheng, A. Hirata, T. Fujita, Z. Tang, M. W. Chen, *Energy Environ. Sci.* **2016**, *9*, 2257–2261.

[9] a) T. F. Jaramillo, K. P. Jørgensen, J. Bonde, J. H. Nielsen, S. Horch, I. Chorkendorff, *Science* **2007**, *317*, 100–102; b) J. Kibsgaard, Z. Chen, B. N. Reinecke, T. F. Jaramillo, *Nat. Mater.* **2012**, *11*, 963; c) A. B. Laursen, S. Kegnæs, S. Dahl, I. Chorkendorff, *Energy Environ. Sci.* **2012**, *5*, 5577–5591; d) Y. Yin, J. C. Han, Y. M. Zhang, X. H. Zhang, P. Xu, Q. Yuan, L. Samad, X. J. Wang, Y. Wang, Z. H. Zhang, P. Zhang, X. Z. Cao, B. Song, S. Jin, *J. Am. Chem. Soc.* **2016**, *138*, 7965–7972; e) L. Wang, X. Liu, J. Luo, X. Duan, J. Crittenden, C. Liu, S. Zhang, Y. Pei, Y. Zeng, X. Duan, *Angew. Chem.* **2017**, *129*, 7718–7722; *Angew. Chem. Int. Ed.* **2017**, *56*, 7610–7614; f) J. Yang, J. Zhu, J. Xu, C. Zhang, T. Liu, *ACS Appl. Mater. Interfaces* **2017**, *9*, 44550–44559; g) J. Yang, K. Wang, J. Zhu, C. Zhang, T. Liu, *ACS Appl. Mater. Interfaces* **2016**, *8*, 31702–31708; h) Y. Li, K. Yin, L. Wang, X. Lu, Y. Zhang, Y. Liu, D. Yan, Y. Song, S. Luo, *Appl. Catal. B* **2018**, *239*, 537–544.

[10] Q. F. Gong, L. Cheng, C. H. Liu, M. Zhang, Q. L. Feng, H. L. Ye, M. Zeng, L. M. Xie, Z. Liu, Y. G. Li, *ACS Catal.* **2015**, *5*, 2213–2219.

[11] a) Q. P. Lu, Y. F. Yu, Q. L. Ma, B. Chen, H. Zhang, *Adv. Mater.* **2016**, *28*, 1917–1933; b) H. Tang, K. P. Dou, C. C. Kaun, Q. Kuang, S. H. Yang, *J. Mater. Chem. A* **2014**, *2*, 360–364.

[12] a) C. Xu, S. J. Peng, C. L. Tan, H. X. Ang, H. T. Tan, H. Zhang, Q. Y. Yan, *J. Mater. Chem. A* **2014**, *2*, 5597–5601; b) V. Kiran, D. Mukherjee, R. N. Jenjeti, S. Sampath, *Nanoscale* **2014**, *6*, 12856–12863; c) V. Klee, E. Preciado, D. Barroso, A. E. Nguyen, C. Lee, K. J. Erickson, M. Triplett, B. Davis, I. H. Lu, S. Bobek, J. McKinley, J. P. Martinez, J. Mann, A. A. Talin, L. Bartels, F. Leonard, *Nano Lett.* **2015**, *15*, 2612–2619; d) X. S. Chen, Z. G. Wang, Y. F. Qiu, J. Zhang, G. B. Liu, W. Zheng, W. Feng, W. W. Cao, P. A. Hu, W. P. Hu, *J. Mater. Chem. A* **2016**, *4*, 18060–18066; e) J. J. Zhang, M. H. Wu, Z. T. Shi, M. Jiang, W. J. Jian, Z. R. Xiao, J. X. Li, C. S. Lee, J. Xu, *Small* **2016**, *12*, 4379–4385; f) L. Yang, Q. Fu, W. H. Wang, J. Huang, J. L. Huang, J. Y. Zhang, B. Xiang, *Nanoscale* **2015**, *7*, 10490–10497.

[13] a) M. Chhowalla, H. S. Shin, G. Eda, L. J. Li, K. P. Loh, H. Zhang, *Nat. Chem.* **2013**, *5*, 263; b) M. A. Lukowski, A. S. Daniel, F. Meng, A. Forticaux, L. S. Li, S. Jin, *J. Am. Chem. Soc.* **2013**, *135*, 10274–10277; c) Y. Yin, Y. M. Zhang, T. L. Gao, T. Yao, X. H. Zhang, J. C. Han, X. J. Wang, Z. H. Zhang, P. Xu, P. Zhang, X. Z. Cao, B. Song, S. Jin, *Adv. Mater.* **2017**, *29*, 1700311.

[14] D. Kong, H. Wang, J. J. Cha, M. Pasta, K. J. Koski, J. Yao, Y. Cui, *Nano Lett.* **2013**, *13*, 1341–1347.

[15] a) M. Acerce, D. Voiry, M. Chhowalla, *Nat. Nanotechnol.* **2015**, *10*, 313; b) L. Cai, J. F. He, Q. H. Liu, T. Yao, L. Chen, W. S. Yan, F. C. Hu, Y. Jiang, Y. D. Zhao, T. D. Hu, *J. Am. Chem. Soc.* **2015**, *137*, 2622–2627.

[16] M. Jiang, J. Zhang, M. Wu, W. Jian, H. Xue, T. W. Ng, C. S. Lee, J. Xu, *J. Mater. Chem. A* **2016**, *4*, 14949–14953.

[17] L. Yang, W. Wang, Q. Fu, J. Zhang, B. Xiang, *Electrochim. Acta* **2015**, *185*, 236–241.

Manuscript received: January 16, 2019
Revised manuscript received: February 17, 2019
Accepted manuscript online: February 18, 2019
Version of record online: March 26, 2019